Performance Investigation of Lab-Scale Sensible Heat Storage System

Chilaka Ravi Chandra Rao, Hakeem Niyas, Likhendra Prasad and Muthukumar Palanisamy

Abstract This paper presents the theoretical investigation of heat storage characteristics and transient behaviour of a sensible heat storage (SHS) module of 10 MJ storage capacity designed for discharging the heat in the temperature range of 523–623 K for solar power plant applications. Thermal model of heat storage module in cylindrical configuration has been developed considering the heat transfer enhancement technique in the storage module by incorporating the axial fins on the discharging tube surfaces. High thermal conductivity (cast iron and cast steel) and low thermal conductivity (concrete) materials have been chosen as the SHS materials for the present analysis. Number of discharging tubes with axial fins over the tube periphery has been optimized based on the charging time.

Keywords Sensible heat storage · Thermal modelling · Concrete · Cast iron · Cast steel

Nomenclature

a	Centre distance between adjacent tubes, (m)
b	Thickness of fins on the HTF tubes, (m)
C_{ps}	Specific heat of SHS material, (J/kg K)
C_{pf}	Specific heat of heat transfer fluid, (J/kg K)
d	Internal diameter of the HTF tubes, (m)
D	Diameter of storage module, (m)
h	Height of fins on the charging tubes, (m)
k_s	Thermal conductivity of SHS material, (W/m K)
L	Length of SHS module, (m)
m	Mass of SHS material, (kg)
n	Number of HTF tubes
n_{fin}	Number of fins on a HTF tube

C.R.C. Rao · H. Niyas · L. Prasad · M. Palanisamy (✉)
Department of Mechanical Engineering, Indian Institute of Technology Guwahati, Guwahati, Assam, India
e-mail: pmkumar@iitg.ernet.in; pmkumariitg@gmail.com

L. Chandra and A. Dixit (eds.), *Concentrated Solar Thermal Energy Technologies*, Springer Proceedings in Energy, https://doi.org/10.1007/978-981-10-4576-9_16

Q	Heat storage capacity, (J)
t	Discharging time, (s)
t_{eff}	Effective discharging time, (s)
T_{ini}	Initial temperature of storage system, (K)
T_{inlet}	HTF inlet temperature, (K)
T_{outlet}	HTF outlet Temperature, (K)
V	Volume of storage material, (m^3)
V_{min}	Minimum volume of storage material required to store 10 MJ, (m^3)
ρ_s	Density of solid-state SHS material, (kg/m^3)
ρ_f	Density of HTF, (kg/m^3)
μ	Dynamic viscosity of HTF, (Ns/m^2)
η_{disch}	Discharging energy efficiency
$\vec{v}$	Velocity of HTF, (m/s)

1 Introduction

Energy saving and development of efficient energy storage systems have been the main objectives especially when the source of energy is intermittent like solar energy. Integration of thermal energy storage (TES) system can enable a constant power generation from solar thermal power plants (STPP). The three main types of TES systems are sensible heat storage (SHS), latent heat storage (LHS) and thermo-chemical heat storage (TCHS) systems. In SHS systems, heat is stored by raising the temperature without causing the phase change of storage medium (liquid or solid). Liquid media (mostly molten salts) is the proven technology for SHS systems but major problems with liquid media system are bulky storage tanks for hot and cold fluids and expensive heat exchangers. Although one tank can be eliminated by using thermocline system [1] but freezing of molten salts at high temperature is still a key problem and the requirement of auxiliary heating units during freezing period leads to higher operating cost. In addition, most of the molten salts become unstable beyond 550 °C [2]. An alternative to liquid media storage is LHS that involves phase transition (i.e. solid to liquid and vice versa) of storage material for storing/releasing heat. LHS technology is in development stage and presently, no commercially large-scale storage heat applications are available.

Fernandez et al. [3] and Khare et al. [2] have shown that concrete, cast iron, and cast steel can be the suitable materials of high temperature SHS application. The TES system using solid-state SHS material is generally employed by set in a multiple tube heat exchanger in the SHS material to transfer the heat from/to the heat transfer fluid (HTF), such as air, molten salt, steam, and thermic oil. The benefits of concrete-based storage systems are the low storage material costs and low degradation of heat transfer between the HTF and concrete [4]. The main requisite properties of SHS material are high heat capacity, density and heat

conductivity. Tamme et al. [5] explored the possibility of employing ceramic and concrete as SHS materials for high temperature heat storage applications. Laing et al. [6] performed the investigation on the SHS system employing ceramic and concrete for 350 kW storage capacity at 663 K. Concrete is selected due to its low exergy loss, low cost and easy handling although ceramic has 35% more thermal conductivity and 20% higher storage capacity. Laing et al. [7] presented the design and test results of a SHS system employing concrete as SHS material and thermic oil as HTF in the temperature range of 573–673 K. For a storage capacity of 400 kWh, the reported charging and discharging times were 6 h. According to John et al. [8], concrete has better resistance to thermal cyclic loading during charging and discharging and could retain its mechanical properties over such cycles. The major issues associated with concrete as a SHS material are the larger size and slower heat transfer rate. However, heat transfer characteristics in low conductivity solid storage media such as concrete, magnesia, etc., can be improved by incorporating heat transfer enhancement techniques [9] and storage module size can be minimized by selecting high thermal capacity materials with high temperature swing. Nandi et al. [10] reported that concrete and castable ceramic are less cost (25–30$ kWh) and durable SHS materials. Sragovich [11] analysed the transient behaviour of SHS system using magnesia as SHS material. It was observed that there always exists a critical mass flow rate of HTF at which the outlet temperature of HTF drops suddenly and this critical value varies in the same fashion as the tube diameter. Miro et al. [12] have tested a by-product of potash industry as a SHS material for its suitability. Anderson et al. [13] predicted the performances of heat storage system employing alumina as the SHS material using compressed air as the HTF.

From the previous reported works, it is seen that most of the researchers [3–5, 7, 8, 10] emphasized the usage of concrete as a SHS material at high temperatures. However, very few works are reported on the heat transfer enhancement studies in solid media storage, although feasibility study has been done. Further, the optimization of the number of HTF tubes used in the solid media storage system is not reported in the literature. It is also important to note that for a given geometry of SHS unit, its heat transfer augmentation techniques also need to be optimized. In the recent studies by the author's research group [14], the charging characteristics of the SHS system employing cast iron, cast steel storage and concrete as the SHS materials were presented. In this study, discharge characteristics of solid-state heat storage systems are analysed employing two high thermal conductivity solid-state SHS materials (cast iron and cast steel) and a low thermal conductivity solid-state SHS material (concrete). Number of HTF tubes and axial fins on the HTF tube is optimized based on the storage module's charging time using COMSOL™ Multi-physics 4.2. The thermal storage performances of the selected SHS materials are predicted for discharging 10 MJ stored heat.

2 Design of Sensible Heat Storage Model

The main aspects considered in the design of storage system are the thermophysical properties and storage temperature range of SHS materials. The design procedures for SHS model are given below:

- Fix the charging temperature range (ΔT_{ch} = 100 K) of storage module.
- Cast iron, cast steel and concrete are selected as SHS materials based on the thermophysical properties, cheaper cost [2, 10] and more availability. Also, the selected SHS materials are modular, i.e. they can be easily implemented for higher heat storage modules. The thermophysical properties of SHS materials, copper and thermic oil are given in Table 1.
- The minimum volume (V_{min}) of SHS material needed for storing 10 MJ of heat is found using Eq. (1).

$$Q = \rho_s V_{min} C_{ps} \Delta T_{ch} \text{ (J)} \tag{1}$$

- Equation (1) can be rewritten as Eq. (2). The values of D^2L for concrete, cast iron and cast steel are 0.06808, 0.03157 and 0.0272, respectively. Now these values are arrived by trial and error technique for different L/D ratios as presented in Table 2.

Table 1 Thermo-physical properties of SHS material [4, 16], copper [17] and thermic oil

Sl. No.	SHS/tube/HTF material	Density (kg/m^3)	Thermal conductivity (W/m K)	Specific heat (J/kg K)	Dynamic viscosity (Ns/m^2)
1	Concrete	2200	1.5	850	–
2	Cast steel	7800	40	600	–
3	Cast iron	7200	37	560	–
4	Copper	8933	401	385	–
5	Thermic oil	761	0.121	2800	0.02

Table 2 Selection of diameter (D) and length (L) of SHS modules

D (m)	D^2 (m^2)	Length (m)				$D^2 * L$(m^3)			
		L/D				L/D			
		1.5	2	2.5	3	1.5	2	2.5	3
0.20	0.04	0.3	0.4	0.5	0.6	0.012	0.016	0.02	0.024
0.25	0.0625	0.375	0.5	0.625	0.75	0.02343	0.03125	0.03906	0.04687
0.30	0.09	0.45	0.6	0.75	0.9	0.0405	0.054	0.0675	0.081
0.35	0.1225	0.525	0.7	0.875	1.05	0.06431	0.08575	0.10718	0.12862
0.40	0.16	0.6	0.8	1	1.2	0.096	0.128	0.16	0.192

$$D^2L = \frac{4Q}{\pi\rho_s C_{ps}\Delta T}\ (\mathrm{m}^3) \tag{2}$$

- It can be observed from Table 2 that the value of D^2L which is close to the required value (0.068087, which is obtained from Eq. 1) of D^2L for concrete is 0.0675 for D = 0.3 m and L/D = 2.5. Therefore, the chosen concrete module's diameter (D) and length (L) are 0.30 and 0.80 m, respectively. Similar methodology is adopted for cast iron and cast steel modules and the required D^2L will be satisfied with D = 0.25 m and L = 0.6 m for both the materials.
- Diameter (d) of the tube is selected as 0.0125 m with a wall thickness of 1.5 mm. Half-inch tube diameter is chosen as it is easily available and also the volume available for heat storage with this size of tube is within limit. Selecting the next standard size, i.e. ¾ or 1 inch would not satisfy the minimum volume criteria. SHS material volume at different standard sizes of tube diameters is tabulated in Table 3.
- Volume of SHS material available for heat storage is estimated using Eq. (3) and it is ensured that this volume is not less than the minimum volume obtained from Eq. (1) for all three materials.

$$V = \left[\frac{\pi}{4}\left(D^2 - nd^2\right) - nn_{\mathrm{fin}}bh\right]L\ (\mathrm{m}^3) \tag{3}$$

- Straight rectangular fins with thickness (b) of 2 mm, height (h) 10 mm and length equal to the storage module are chosen.

Table 3 Selection of tube diameter (d) as per standard size availability for SHS concrete module

Diameter of the module, D (m)			0.2	0.250	0.30	0.350	0.4
Length of the module, L (m)	L/D = 1.5		0.3	0.375	0.45	0.525	0.6
	L/D = 2		0.4	0.500	0.60	0.700	0.8
	L/D = 2.5		0.5	0.625	0.75	0.875	1.0
	L/D = 3		0.6	0.750	0.90	1.050	1.2
Available volume of the module, $V \times 10^{-3}$ (m^3)	L/D 1.5	d (1/2″)	8.269	16.96	30.08	48.49	73.09
		d (3/4″)	7.387	15.86	28.75	46.94	71.32
		d (1″)	6.171	14.34	26.93	44.82	68.89
	L/D 2	d (1/2″)	11.03	22.62	40.10	64.65	97.45
		d (3/4″)	9.849	21.15	38.34	62.59	95.10
		d (1″)	8.228	19.12	35.90	59.76	91.85
	L/D 2.5	d (1/2″)	13.78	28.27	50.13	80.82	121.8
		d (3/4″)	12.31	26.43	47.92	78.24	118.9
		d (1″)	10.29	23.90	44.88	74.69	114.8
	L/D 3	d (1/2″)	16.54	33.93	60.15	96.98	146.2
		d (3/4″)	14.77	31.72	57.50	93.89	142.6
		d (1″)	12.34	28.68	53.86	89.63	137.8

Table 4 Estimated mass of SHS material

SHS material	D (m)	L (m)	V_{min} from Eq. (1) (m^3)	V from Eq. (2) (m^3)	m (kg)	m with 20% margin (kg)
Concrete	0.30	0.8	0.0535	0.0535	118	142
Cast iron	0.25	0.6	0.0214	0.029	230	276
Cast steel	0.25	0.6	0.0248	0.029	212	254

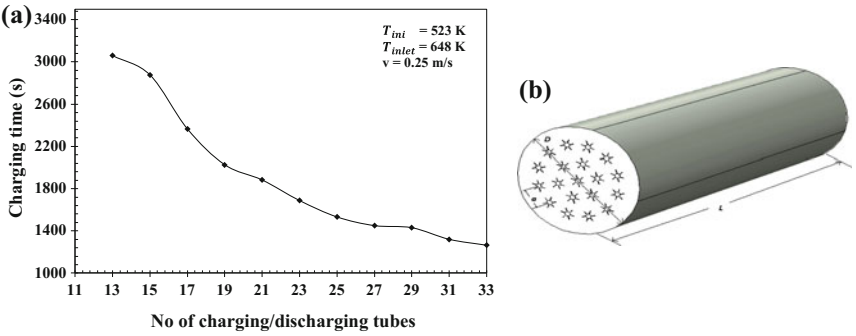

Fig. 1 **a** Optimization of the number of HTF tubes, **b** optimized thermal model of 10 MJ capacity [14]

Storage volume of the module is calculated considering copper fins on the discharging tubes. Based on the above calculation, the mass of SHS material with a factor of safety of 1.2 on actual available mass (obtained from Eq. 3) is given in Table 4.

2.1 Optimization of the Number of HTF Tubes of the SHS Module

Decreasing the number of HTF tubes (n) increases the charging/discharging time considerably but also improves the SHS capacity slightly. Hence, to optimize the number of HTF tubes, the charging times with respect to the different arrangements of HTF tubes are presented in Fig. 1a. From Fig. 1a, it can be seen that there are two ranges of tube arrays at which the charging time does not vary significantly [14]. First range of charging tube array lies between 19 and 21 tubes with the charging time difference of 72 s and second range of 27–29 tubes with the charging time difference of about 20 s. If the second range of tubes is selected, then the charging time of the storage module reduces by 10 min approximately. At the same time, it incurs additional cost of 8–10 tubes and also reduces the effective storage

volume below the minimum storage volume (from Eq. 1) required for storing 10 MJ of heat. Thus, as shown in Fig. 1b, the number of HTF tubes in the optimum module configuration is selected as 19.

3 Thermal Modelling of Sensible Heat Storage Module

3.1 Model Description

The storage module acts like a heat exchanger that releases/absorbs heat energy when the cold/hot HTF is passed through the HTF tubes/holes. It consists of a cylindrical module with finned tubes embedded into concrete module (Fig. 1b). For cast iron and cast steel, simply holes/drills are made. Three-dimensional conjugate heat transfer model of cylindrical storage module which includes 3D solid and 3D fluid domains has been considered in the present study. In order to minimize the computational time and cost, one-fourth of the storage module has been selected as the heat transfer is symmetrical (shown in Fig. 2 for concrete module). During discharging of heat from module, HTF is supplied at lower temperature to the storage module from one end and it leaves from the other end. While passing through the tubes, HTF absorbs the heat energy from the charged storage module through the mode of conjugate heat transfer. The details of physical model of 10 MJ SHS system are already reported by the authors [14].

3.2 Governing Equations

In this section, a summary of thermal model employed for simulating the transient behaviour of the SHS module is presented. The assumptions employed in the thermal model are: (i) HTF inlet velocity profile is fully developed, (ii) SHS module material is isotropic and no axial conduction in the HTF, (iii) outer surface of the cylinder is well insulated, and thus it is adiabatic and (iv) neglected radiation effects. Cast iron and cast steel modules have zero contact resistance as these metallic modules have drilled holes and direct heat transfer takes place between

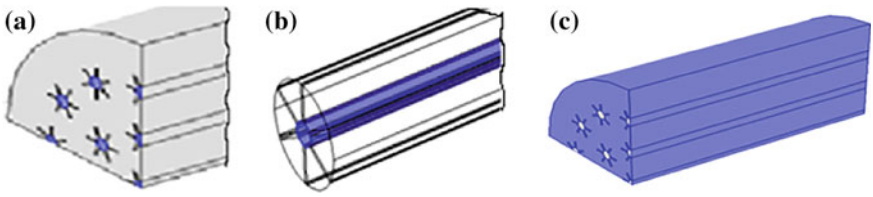

Fig. 2 Initial condition **a** at inlet, **b** no slip boundary condition at interface of a tube and **c** thermal insulation boundary condition [14]

HTF and cast iron or cast steel module. In case of concrete module, the contact resistance is neglected as the charging tubes are buried inside the concrete module.

The governing equations for the fluid flow and heat transfer between the HTF and SHS module are as follows:

Fluid flow

$$\nabla \cdot \vec{v} = 0 \tag{4}$$

$$\rho_f \frac{D\vec{v}}{Dt} = -\nabla P + \mu \nabla^2 \vec{v} \tag{5}$$

Convection: Solid-liquid interface

$$\rho_f C_{pf} \frac{DT}{Dt} = k_s \nabla^2 T \tag{6}$$

Conduction: Solid region

$$\rho_s C_{ps} \frac{\partial T}{\partial t} = k_s \nabla^2 T \tag{7}$$

3.3 Initial and Boundary Conditions

Initially, at inlet (t = 0), there is no HTF flow through the tubes (i.e. at rest). All the domains are also initially assigned a constant temperature of T_{ini}. The discharge process is commenced by specifying a constant fluid inlet temperature of T_{inlet} and a constant fluid velocity. Except the inlet and outlet, all the other surfaces are insulated. Figure 2a–c illustrates the initial and boundary conditions of 3D cylindrical storage module model [14, 15].

Inlet:

$$\begin{aligned} &\text{At } (t = 0) : \vec{v} = 0; \quad T = T_{\text{ini}} \\ &\text{At } (t > 0) : \vec{v} \neq 0; \quad T = T_{\text{inlet}} \end{aligned}$$

Interface:

$$\text{No slip } (\vec{\text{v}} = 0)$$

At the solid–liquid Interfaces.

Thermal insulation:

$$n \cdot (k \nabla T) = 0;$$

where, n is the normal vector.

3.4 Performance Parameters

The performance parameters are discharging time, effective discharging time (for concrete), energy recovered and discharging energy efficiency. These parameters are useful to evaluate the transient performance of the storage modules during the discharge process. Complete discharging time is the time taken by the storage module's average volume temperature to attain the HTF inlet temperature, T_{inlet}. Effective discharging time is the time at which the temperature difference between the storage module's volume average temperature and the outlet temperature of the HTF becomes 5 °C, i.e. for maintaining better heat transfer rate between the storage module and heat transfer fluid, at least 5 °C temperature difference is recommended due to less thermal conductivity of concrete. The amount of heat retrieved from the storage module is calculated using Eq. (8).

$$Q = \rho_s V C_{ps}(T\text{ini} - T(t)), \tag{8}$$

where T_{ch} is the volume average temperatures of module at the end of charging cycles.

Discharging energy efficiency is the ratio of the energy released during the discharging cycle to the maximum energy that can be recovered from the storage module as applied in case of charging energy efficiency [16]

$$\eta_{\text{disch}} = \frac{T_{\text{ini}} - T(t)}{T_{\text{ini}} - T_{\text{inlet}}} \tag{9}$$

3.5 Grid Independence Test

Comparisons are made for results obtained from different mesh densities for the concrete module configuration to make sure that the results are mesh independent. The range of the densities is varied from 43,969 to 139,438 elements with three different mesh profiles at the predefined temperatures (shown in Fig. 3). The three grid profiles are extremely coarse (43,969 elements), extra coarse (67,667 elements) and coarser (139,438 elements). As illustrated in Fig. 3, the results obtained from the mesh sizes of 67,665 (extra coarse) and 139,438 (coarser) matched closely. It is also noted that increasing the mesh elements beyond coarser mesh (fine mesh 269,000) leads to an increase in computational time by about 30 h. In order to save the computational time, mesh size of 67,665 has been chosen for the further analysis. The governing equations are solved using the time-dependent PARADISO solver. The simulations are carried out using Intel (R) Core™ i5-2400CPU@3.10 GHz machine (installed memory of 8 GB) with a time stepping of 0.1 s.

3.6 Validation of Current Model

To validate the developed thermal model, the obtained numerical results (charging time) of the storage module at different thermal conductivity values are compared with the data reported by Tamme et al. [5]. The initial and boundary conditions, thermophysical property of the SHS module selected for the numerical validation are taken from Tamme et al. [5]. It is understood from Fig. 4 that the numerical results predicted for the current model showed a good agreement with the data reported by Tamme et al. [5]. However, at the initial period of charging, a small deviation was observed which might be due to neglecting the axial conduction in HTF.

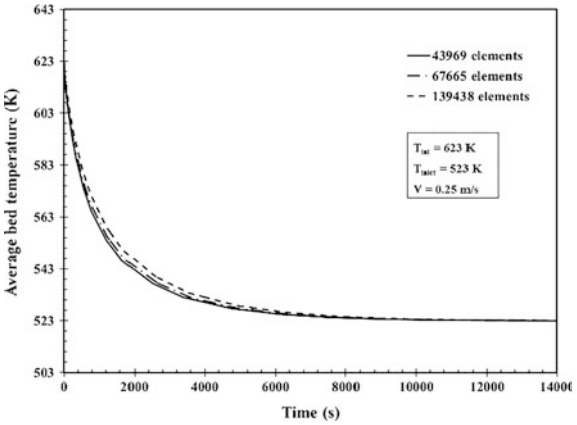

Fig. 3 Grid independent test for the concrete module

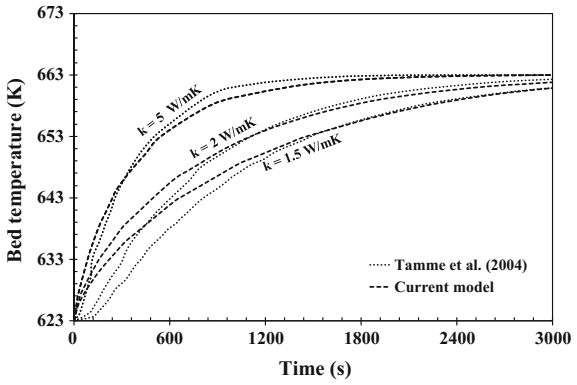

Fig. 4 Validation of the numerical model [14]

4 Results and Discussion

In the following section, some of important numerical results obtained from the simulation are presented.

4.1 Discharging Time

Storage module is said to be discharged completely when its volume average temperature reaches almost the inlet temperature of HTF. Figure 5a shows the complete discharging time of the concrete storage module. The complete discharging time of the charged concrete unit is about 13,965 s. It can be found that the temperature drop of the concrete module is fast for the first 3600 s due to higher potential of conduction. This driving potential decreases gradually due to lower difference in temperature between the HTF and the storage module. As the time progresses beyond 5050 s, the slope of discharging curve becomes flat. Therefore, considering the minimum temperature difference of 5 °C between average storage module's temperature and HTF outlet temperature (required for effective heat

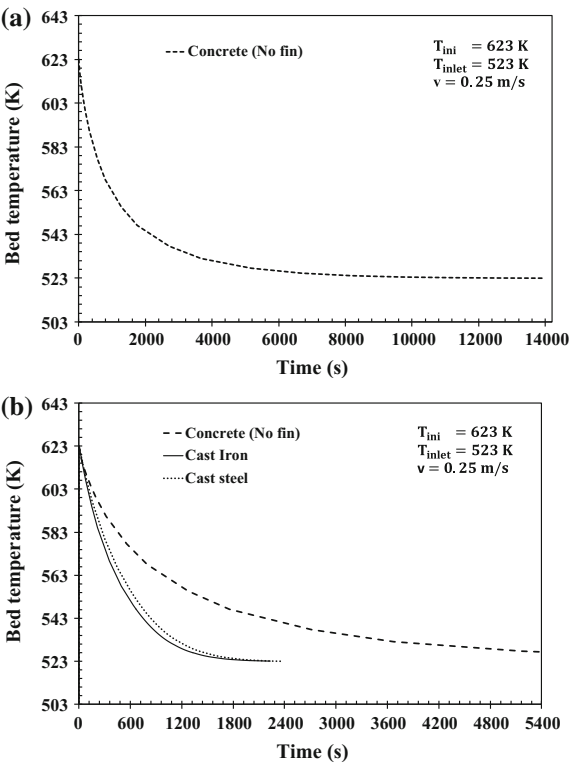

Fig. 5 Discharging time of **a** concrete (complete) and **b** concrete (effective), cast iron and cast steel modules

transfer), 5050 s is considered as the effective discharging time for concrete storage module provided the energy that is recovered is at least 10 MJ. It has been found that the energy recovered at 5050 s is within the limit of the design capacity, which is discussed in next section. The effective discharging time of concrete module and complete discharging time of cast iron and cast steel modules are shown in Fig. 5b. The complete discharging time of the cast iron and cast steel modules is 1728 and 1887 s, respectively.

4.2 Thermal Energy Discharged from the Storage Modules

Figure 6 shows the discharge rate of the thermal energy from the selected SHS materials. The amount of heat discharged from the different SHS modules at their respective discharging times (i.e. effective time for concrete module and complete time for metallic modules) is calculated using Eq. (8). Thermal energy discharged from concrete, cast iron and cast steel storage modules are 12.11, 14.24 and 16.51 MJ, respectively within 5050, 1728, and 1887 s.

4.3 Discharging Energy Efficiency (DEE)

Discharging energy efficiencies of the three selected storage materials are shown in Fig. 7. For the cast iron and the cast steel storage materials, DEE is almost about 100% because the average volume temperature of these storage modules attains the value of the T_{inlet} within their respective discharging times. While the concrete storage module is being less heat conductive, its volumetric temperature does not reach the T_{inlet} within the discharging time of 5050 s. The discharging energy efficiency of the concrete storage module is about 95%.

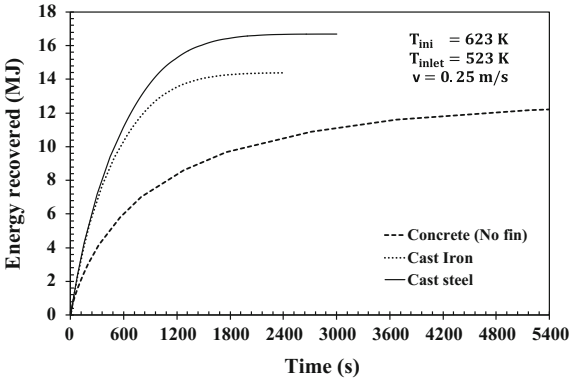

Fig. 6 Thermal energy discharge rate from SHS modules

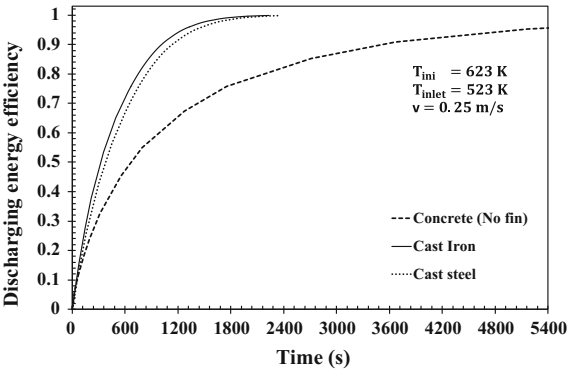

Fig. 7 Discharging energy efficiency of SHS modules

4.4 Axial Variation of HTF Temperature

Initially, the storage module is fully charged and its average volume temperature is 623 K. When the discharging process is initiated by supplying HTF at temperature 523 K, the heat stored in the storage module is transferred to the discharging tube, which is further carried away by HTF through convection. As the HTF moves along the module (axial direction), its temperature rises and exits at a temperature much higher than its inlet temperature. In order to analyse the axial variation of HTF temperature, temperature at an interval of every 10 cm along the axial direction is predicted. It can be noticed that the HTF temperature rise is rapid for the early period of discharging process and after a certain time no appreciable temperature rise is seen as the storage module temperature itself decreases with time resulting into the retardation of driving potential for conduction. The rise in HTF temperature is more significant in cast iron and cast steel as compared to concrete module. For example, the rise in HTF temperature predicted in concrete, cast iron and cast steel module, during the discharging time of 1 min are about 21, 63 and 66 K, respectively. These effects are shown in Fig. 8a–c, for cast iron, cast steel and concrete, respectively. For all the three storage materials, the HTF temperature rise is significant up to 30 min.

4.5 Effect of Fins on Discharging Time

For achieving better heat transfer rate, the effective thermal conductivity of the concrete is enhanced by adding the fins on the outer surface of charging/discharging tubes. In order to account the effect of fins, the discharging time of concrete storage module without fins is compared with finned tube concrete storage module. It is noticed from Fig. 9 that the incorporation of fins on tubes causes the considerable enhancement in heat conduction in the concrete storage module and hence the total discharging time of the storage module is reduced significantly. The reduction in

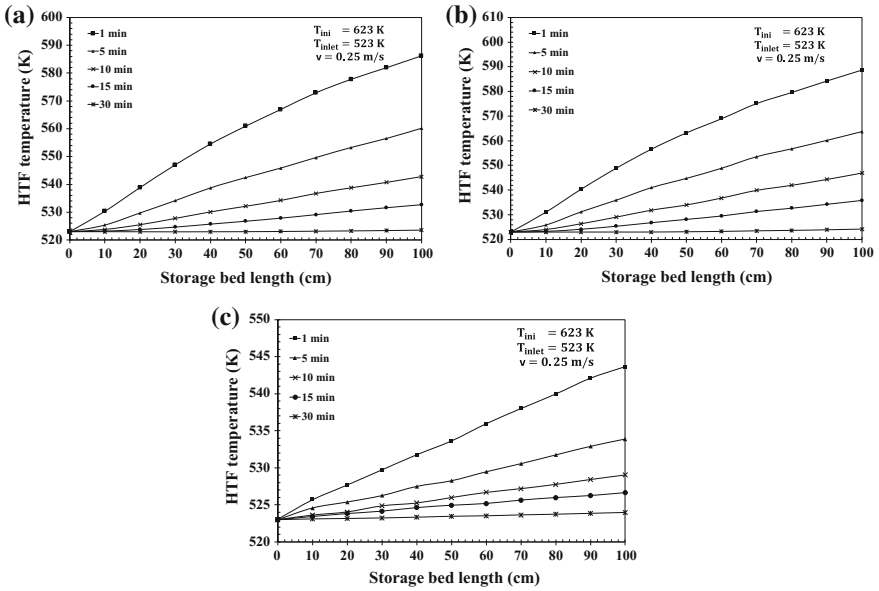

Fig. 8 Axial variation of HTF temperature in the storage module at different time intervals **a** cast iron, **b** cast steel and **c** concrete (no fin)

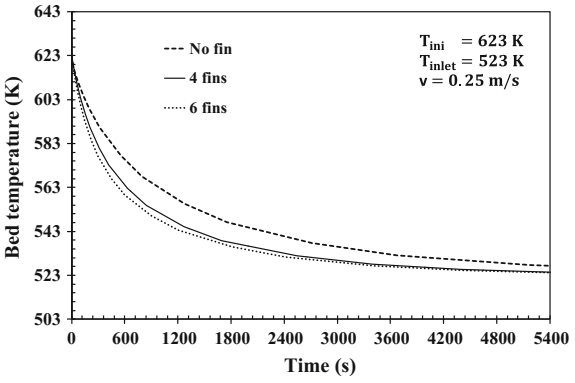

Fig. 9 Effect of number of fins on discharging time of concrete module

effective discharging times are about 32.2 and 35.9% for the tubes with four fins and six fins cases in comparison with the concrete module without fin. Further increasing the number of fins would not satisfy the minimum volume criteria for required heat storage and it is also uneconomic. Thus for discharging cycle, tube with four fins gives the optimum discharging time.

4.6 Effects of Fins on Energy Recovered

Figure 10 shows the effect of the number of fins on the thermal energy recovered from the storage modules. Although the addition of fins on tubes reduces the volume of concrete marginally but the reduction in the discharging time is very significant. With addition of fins on a discharging tube of concrete module, the reductions in energy discharged from concrete module are 1.7 and 2.6% for four fins and six fins, respectively. Table 5 provides the effect of number of fins on the complete and effective discharge times of the concrete module and the respective heat discharge capacities.

4.7 Effect of HTF Velocity on Discharging Time

Increasing the HTF velocity causes the improvement in the overall heat transfer coefficient, which accelerates the rate of temperature drop of storage module. Hence, it takes less time to reach the T_{inlet} resulting in the reduction of the discharging time. The variation in HTF inlet velocity on the discharging time for concrete with four fins, cast iron and cast steel are shown in Fig. 11a, b. The

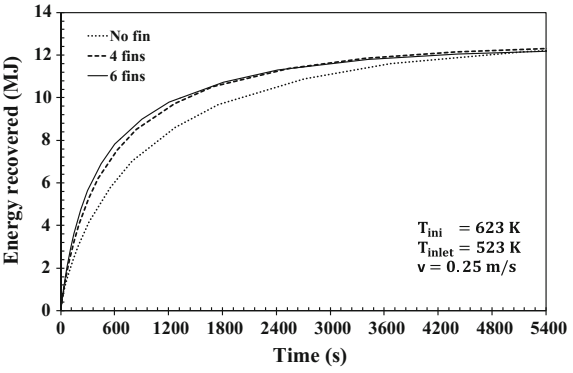

Fig. 10 Effect of number of fins on energy recovered from concrete module

Table 5 Effect of the number of fins on the complete and effective discharge times of the concrete module and the respective heat discharge capacities

n_{fin}	Discharging time (s)		Energy discharged (MJ)		Corresponding storage module temperature (K)
	t_{eff}	t	Effective energy discharged	Complete energy discharged	
0	5050	13,965	12.11	12.74	528
4	3423	9649	11.87	12.48	528
6	3238	9165	11.71	12.31	528

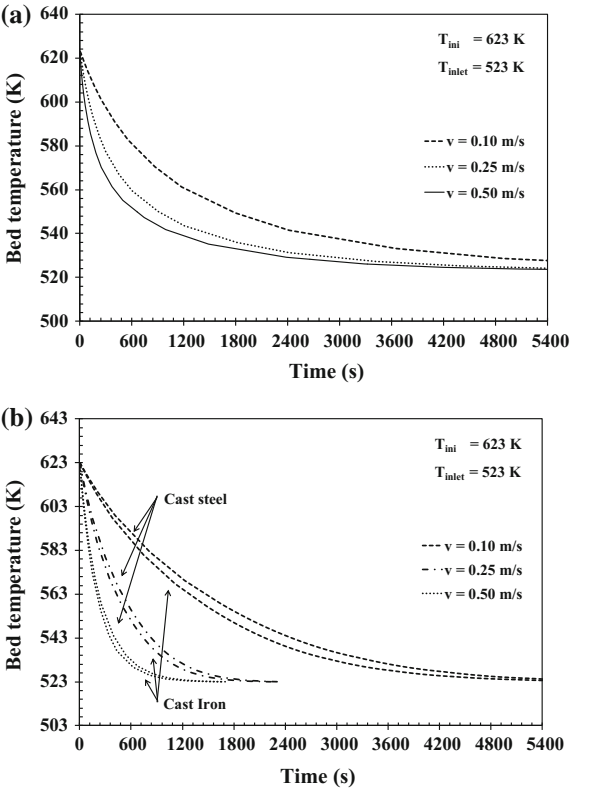

Fig. 11 Effect of HTF velocity on the discharging time of the SHS modules **a** concrete, **b** cast steel and cast iron

effective discharging time of concrete (with four fins) SHS module for velocity of 0.1, 0.25 and 0.5 m/s are 5334, 3423 and 2435 s, respectively. Similarly, the complete discharging time of cast iron and cast steel modules for the corresponding velocities are 5145, 1728 and 1110 s, and 5626, 1887 and 1197 s respectively. The reduction in the discharging time of the SHS module with the case having a HTF velocity of 0.25 m/s when compared to the case with 0.1 m/s is significant but same is not true for the case with a velocity of 0.25 m/s when compared to the case with 0.5 m/s. Further increase in the HTF fluid velocity will not help in reducing the discharging time. Therefore, HTF velocity considered for the current study is 0.25 m/s.

5 Conclusions

Simulated results of SHS system during discharging cycle are presented for three storage materials, viz. concrete, cast iron and cast steel. Heat transfer enhancement technique is implemented by adding fins on the HTF tubes. The effect of

improvement in thermal conductivity of storage module with addition of axial fins on the surface of HTF tubes is analysed for three cases, i.e. tubes with no fins, tubes with four fins and six fins. It is found that the concrete with four fins provided the optimum discharging time with acceptable storage capacity (11.87 MJ) against the designed capacity of 10 MJ. Addition of fins reduces the effective storage volume of concrete; however, the reduction in storage material volume is not significant as compared to decrement in discharging time. Increasing the heat transfer fluid flow rate beyond 0.25 m/s is not significant for all three SHS modules.

Acknowledgements The authors sincerely thank the Department of Science and Technology (DST), Government of India, for the financial support (Project No: DST/TM/SERI/2K10/53(G)).

References

1. Z. Yang, S.V. Garimella, Thermal analysis of solar thermal energy storage in a molten salt thermocline. Sol. Energy **84**, 974–985 (2010)
2. S. Khare, C. Knight, S. McGarry, Selection of materials for high temperature sensible energy storage. Sol. Energy Mater. Sol. Cells **115**, 114–122 (2013)
3. A. Fernandez, M. Martinez, M. Segarra, I. Martorel, F. Cabeza, Selection of materials with potential in sensible thermal energy storage. Sol. Energy Mater. Sol. Cells **94**, 1723–1729 (2010)
4. A. Gil, M. Medrano, F. Cabeza, State of the art on high temperature thermal energy storage for power generation, Part 1—concepts, materials and modellization. Renew. Sustain. Energy Rev. **14**, 31–55 (2010)
5. R. Tamme, D. Laing, W.D. Steinmann, Advanced thermal energy storage technology for parabolic trough. J. Sol. Energy Eng. **126**, 794–800 (2004)
6. D. Laing, W.D. Steinmann, R. Tamme, C. Richter, Solid media thermal storage for parabolic trough power plants. Sol. Energy **80**, 1283–1289 (2006)
7. D. Laing, C. Bahl, T. Bauer, D. Lehmann, Thermal energy storage for direct steam generation. Sol. Energy **85**, 627–633 (2011)
8. E. John, W.M. Hale, R.P. Selvam, Development of a high-performance concrete to store thermal energy for concentrating solar power plants, in *Proceedings of the ASME 5th ICES Washington*, DC, USA (2011)
9. F. Agyenim, P. Eames, M. Smyth, Heat transfer enhancement in medium temperature thermal energy storage system using a multi tube heat transfer array. Renew. Energy **35**, 198–207 (2012)
10. B.R. Nandi, S. Bandyopadhyay, R. Banerjee, Analysis of high temperature thermal energy storage for solar power plant, in *IEEE Third International Conference on Sustainable Energy Technologies*, Nepal (2012)
11. D. Sragovich, Transient analysis for designing and predicting operational performance of a high temperature sensible thermal energy storage system. Sol. Energy **43**, 7–16 (1989)
12. L. Miro, M.E. Navarro, P. Suresh, A. Gil, A.I. Fernandez, L.F. Cabeza, Experimental characterization of a solid industrial by product as material for high temperature sensible thermal energy storage (TES). Appl. Energy **113**, 1261–1268 (2014)
13. R. Anderson, S. Shiri, H. Bindra, J.F. Morris, Experimental results and modelling of energy storage and recovery in a packed bed of alumina particles. Appl. Energy **119**, 521–529 (2014)
14. L. Prasad, P. Muthukumar, Design and optimization of lab-scale sensible heat storage prototype for solar thermal power plant application. Sol. Energy **97**, 217–229 (2013)

15. H. Niyas, L. Prasad, P. Muthukumar, Performance investigation of high-temperature sensible heat thermal energy storage system during charging and discharging cycles. Clean Technol. Environ. Policy **17**, 501–513 (2015)
16. M.Y. Haller, C. Cruickshank, W. Streicher, S.J. Harrison, E. Anderson, S. Furbo, Methods to determine stratification efficiency of thermal storage processes—review and theoretical comparison. Sol. Energy **83**, 1847–1860 (2009)
17. Y. Tian, C.Y. Zhao, A review of solar collectors and thermal energy storage in solar thermal applications. Appl. Energy **104**, 538–553 (2013)